Temporal coherence of propagating surface plasmons

Wang Tao, Geneviève Comtet, Eric Le Moal, Gérald Dujardin, Aurelien Drezet, Serge Huant, Elizabeth Boer-Duchemin

To be published in Optics Letters:

Title:	Temporal coherence of propagating surface plasmons
Authors:	Elizabeth Boer-Duchemin, Geneviève Comtet, Eric Le Moal, Gérald Dujardin, Serge Huant, Aurelien Drezet, and TAO WANG
Accepted:	27 October 2014
Posted:	27 October 2014
Doc. ID:	223941

Temporal coherence of propagating surface plasmons

Tao Wang,[1] Geneviève Comtet,[1] Eric Le Moal,[1] Gérald Dujardin,[1]
Aurélien Drezet,[2] Serge Huant,[2] and Elizabeth Boer-Duchemin[1,*]

[1] *Institut des Sciences Moléculaires d'Orsay (ISMO), CNRS Université Paris-Sud, Orsay, France*
[2] *Institut Néel, CNRS Université Joseph Fourier, Grenoble, France*

compiled: October 24, 2014

The temporal coherence of propagating surface plasmons is investigated using a local, broadband plasmon source consisting of a scanning tunneling microscope. A variant of Young's experiment is performed using a sample consisting of a 200 μm-thick gold film perforated by two 1-μm diameter holes (separated by 4 or 6 μm). The resulting interference fringes are studied as a function of hole separation and source bandwidth. From these experiments we conclude that apart from plasmon decay in the metal, there is no further loss of plasmon coherence from propagation, scattering at holes or other dephasing processes. As a result, the plasmon coherence time may be estimated from its spectral bandwidth.

OCIS codes: (240.6680) Surface plasmons; (030.1640) Coherence; (260.3160) Interference

Coherence is a fundamental property of oscillating fields that has led to exciting physics and important applications in such diverse areas as astronomy and medical imaging. Surface plasmon polaritons (SPPs)—collective oscillations of surface electrons coupled to an electromagnetic wave—are in turn being studied for their potential applications at the nanoscale. While the quantum interference[1–4] and the spatial coherence[5–10] of surface plasmons have been investigated recently, the *temporal* coherence of propagating surface plasmons has been relatively ignored.

Temporal coherence is related to the ability of a wave to interfere with a slightly delayed version of itself, and it is intimately connected to the bandwidth (spectrum) of the wave in question[11]. A monochromatic point source incident on a pair of closely spaced holes will give rise to a fringe pattern with a visibility V of 1, even if a time delay is introduced for light entering or exiting one of the holes[12]. If the spectrum is broadband, however, the resulting phase delay for each frequency component leads to a slightly different fringe pattern, and the combination of these greatly reduces (or even suppresses) the observed visibility away from the center of the fringe pattern. Thus in order to investigate the temporal coherence of propagating surface plasmons, and study whether there is any loss of coherence due to SPP propagation, scattering or other dephasing processes, a wide band source of plasmons must be used.

In this letter, we use a scanning tunneling microscope (STM) to excite broadband propagating surface plasmons on a thick gold film in order to study the SPP temporal coherence properties. The STM is an excellent (quasi-)point source of polychromatic propagating surface plasmons, and produces an out-going circular broadband surface plasmon polariton wave with a dispersion curve typical of that which is found for SPPs on metal films[10, 13, 14]. In this work, we perform a variant of Young's double slit experiment, using a gold film perforated by two 1 μm-diameter holes. The geometry of the experiment is such that the STM-excited plasmon wave is partially scattered into photons at one hole while the rest propagates to and is scattered into photons at the second hole. The scattered photons form interference fringes in the back focal plane which are studied and analyzed as a function of source bandwidth and hole spacing, leading to the conclusion that apart from the effect of losses in the metal, there is no change in coherence upon scattering, propagation, or from other dephasing processes[15, 16].

Figure 1 a) shows a sketch of the experiment. The STM excites an outgoing circular plasmon wave on the sample which consists of a 200 nm-thick (i.e., opaque) gold film on glass in which 1 μm-diameter hole pairs have been realized using focused ion beam etching. Hole pairs with hole separations of 4 and 6 μm are used. When the propagating surface plasmons interact with the holes in the sample, they are scattered into (in-plane) plasmons and (out-of-plane) photons. These photons are collected through the transparent glass substrate and are focused, using the optics of an inverted optical microscope, on a charge-coupled device (CCD) camera. With this setup (described in detail elsewhere[13]) real plane (spatial distribution) and Fourier or back focal plane (angular distribution) images as well as spectra of the emitted light are acquired. The STM parameters used are I_{tunnel}= 6 nA and V_{sample}= 2.8 V.

* Corresponding author: Elizabeth.Boer-Duchemin@u-psud.fr

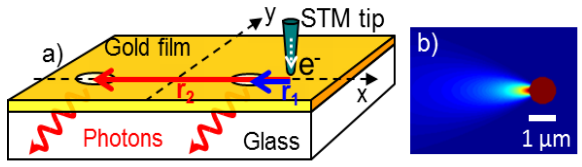

Fig. 1. The experiment. a) The STM tip excites an outgoing circular surface plasmon wave on a 200 nm-thick gold film. The SPP wave travels a distance r_1 or r_2 respectively before encountering the first or second of two 1 μm-diameter holes in the film. At the holes the plasmons are scattered a) into photons which are collected in the far field through the transparent substrate and b) into plasmons. Part b) of the figure is a simulation which shows that plasmon-to-plasmon scattering at 1 μm-diameter holes is strongly in the forward direction. (The STM tip is located to the right of the hole and only the scattered field is represented.)

The SPP excitation position is explicitly chosen to be along the axis formed by the two holes in this work in order to study the temporal coherence of the SPPs (see Fig. 1 a)). The excited plasmon wave that is incident on the first hole is scattered into both (out-of-the-plane) photons and (in-plane) plasmons by the hole; the secondary plasmon wave then propagates to and is scattered into photons (and plasmons) at the second hole. The interfering light thus originates from the STM-excited plasmon wave and a slightly delayed version of itself. An analytical calculation of the plasmon fields modeling the hole as a series of horizontal dipoles whose amplitudes and phases depend on the incident plasmon field[10, 17] shows that the plasmon-to-plasmon scattering at the 1 μm hole is strongly peaked in the forward direction (see Fig. 1 b)).

If there is a fixed phase relationship between the light scattered at the two holes, interference fringes are expected in the Fourier plane. The visibility of these fringes ($V = \frac{I_{max}-I_{min}}{I_{max}+I_{min}}$, with I_{max} and I_{min} equal to the maximum and minimum intensities of neighboring fringes) is related to the coherence of the source. Figure 2 shows the resulting fringe pattern when the STM excitation position is 1 μm from the nearest hole. The fringe spacing is directly related to the distance separating the two holes, as expected in a typical Young's double slit experiment. The maximum of intensity is not located in the center of the image since plasmons are strongly forward scattered into photons at 1 μm-diameter holes[10]. In parts a) to d), a 13 nm-wide bandpass filter centered at 700 nm is placed before the CCD camera, thus greatly narrowing the typical STM-excited plasmon emission spectrum on gold (see the blue curve in Fig. 3). Despite the relative narrowness of the spectrum detected by the CCD, the visibility is seen to be less than unity.

Parts e) to h) of Fig. 2 show the resulting fringe pattern when the full spectrum of Fig. 3 is collected on the CCD camera. Surprisingly, despite the approximately

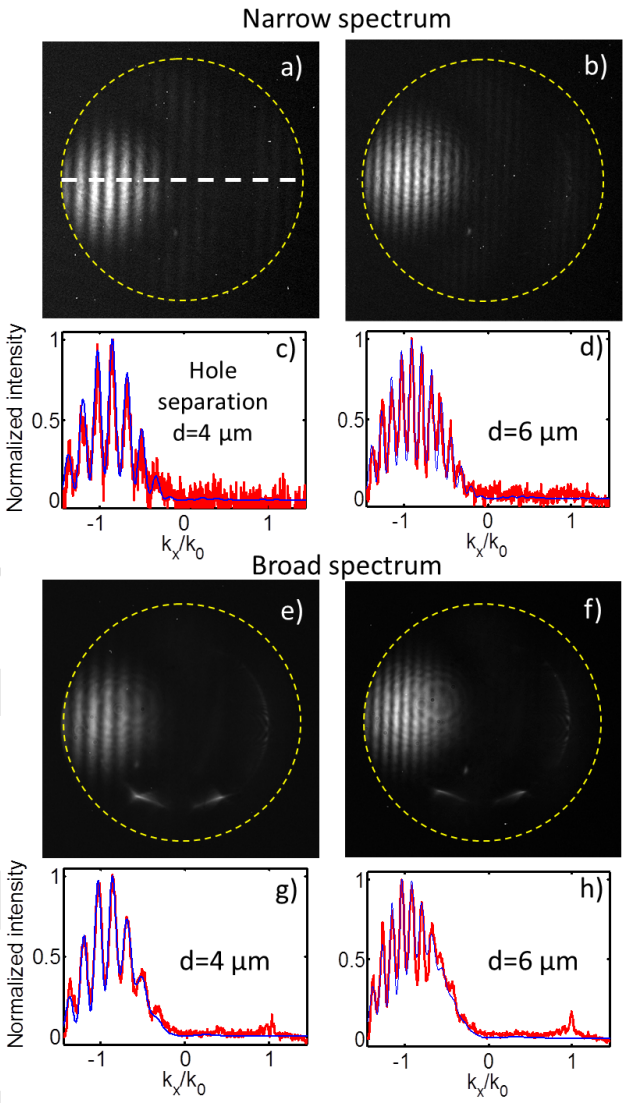

Fig. 2. Interference fringes for STM-excited plasmons scattered into photons at two 1 μm-diameter holes in a 200 nm-thick Au film, in the geometry of Fig. 1. The left and right-hand columns show data from hole pairs separated by 4 and 6 μm respectively; the fringe period observed in the Fourier plane is equal to λ/d where λ is the central wavelength of the emitted radiation and d is the hole separation, as expected for a Young's double slit experiment. For smaller values of d, the hole separation, the fringe spacing increases and the effects of temporal coherence become less obvious. The yellow circle represents the numerical aperture of the collection objective (NA= 1.45). In parts a) and b) (and for the corresponding cross-sections c) and d); the white line in a) shows where the cross-section is obtained), a narrow bandpass filter (width 13 nm, center wavelength 700 nm) is placed before the collecting CCD camera, thus greatly reducing the spectral width of the collected light (see the dotted lines in Fig. 3). For parts e) to h), the collected wavelength range is the same as that of Fig. 3 (i.e., ~450-775 nm). The faint circle and two spots at the bottom of parts e) and f) are artifacts. Note that the signal to noise ratio is lower for the filtered case, as less signal is collected. The red curves are the experimental data, the well-fitting blue curves are the results of the simulation (spectral width in the model is the same as that of the blue curve of Fig. 3).

tenfold increase in the spectral width, there is only a slight decrease in the observed visibility as compared to the filtered case. This could be due to different scattering angles for plasmons of different wavelengths. To test this hypothesis, a similar experiment is carried out but using a single hole and a series of bandpass filters in front of the CCD camera. The data is shown in Fig. 4. No significant difference in scattering angle is observed for plasmons of different energy. Instead, a simple model that takes into account the different phase delays may explain the unexpectedly high visibility achieved with a broad spectrum.

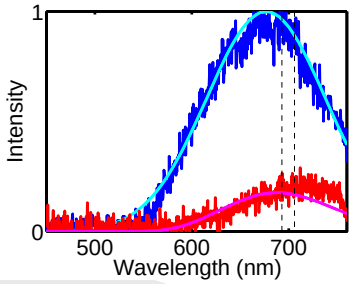

Fig. 3. Simultaneously measured spectra from hole 1 (closest hole, blue curve) and hole 2 (hole furthest from the STM, red curve) and the corresponding fitted (cyan) and calculated (magenta) curves, for two holes separated by 6 μm. The decrease in scattered intensity at the second hole and the wavelength shift of this spectrum towards longer wavelengths are both consistent with a model where these changes are attributed to the wavelength-dependent losses of energy to the Au film during SPP propagation, as confirmed by the calculated curve. The emission spectrum at hole 1 (blue curve) may be fitted with a Gaussian with a full-width-at-half maximum of about 144 nm. The dashed lines around 700 nm represent the spectral range used in parts a) to d) of Fig. 2.

In this experiment, where the STM-excited plasmon wave is first scattered into photons at one hole then at the other, *two* separate components leading to a phase difference between the scattered photons must be considered: the "traditional" Young's double slit phase shift, $k_x d$, which depends on the hole spacing, d, and photon wavevector, k_x, and a second phase shift due to the *plasmon* path difference on the surface, $r_2 - r_1$, and the plasmon wavevector, k'_{SPP}. The fact that the light is scattered at large angles must also be taken into account. This may be modeled in the following way.

For a single wavelength, the intensity along the x-axis in the Fourier plane may be written:

$$I(k_x) = \left(\frac{J_1(u)}{u}\right)^2 \Big[I_1 + I_2 + 2\sqrt{I_1 I_2}\cos\left(k_x d + k'_{SPP}(r_2 - r_1)\right)\Big] \quad (1)$$

with $u = (k_x + k_x^{max})a$; k_x is the component of the photon wavevector that is parallel to the hole axis; k_x^{max} is a experimentally determined parameter representing the position of the maximum intensity of the fringe pattern due to the forward scattering of the radiation; a the radius of the holes; J_1 is the first order Bessel function[17]; I_1 the intensity of the light from hole 1; I_2 the intensity of the light from hole 2; d the hole separation; k'_{SPP} the real part of the plasmon wavevector and r_1 and r_2 the distance from the tip to the first and second hole respectively. The Bessel function term is due to the diffraction of the light by the circular holes.

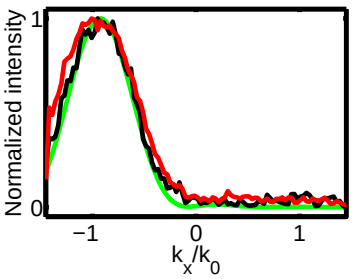

Fig. 4. Fourier plane cross-sections of the emission of STM-excited plasmons scattered into photons at a *single* 1 μm-diameter hole, for different wavelength ranges. The red curve is the data obtained using a bandpass filter centered at 794 nm (bandwidth 160 nm) and the black curve arises from data collected with a bandpass filter centered at 630 nm (bandwidth 92 nm). No significant differences are observed between these two curves, demonstrating that the scattering angle does not substantially depend on the emission wavelength. The green curve is the theoretical curve obtained from equation 2 with $I_2 = 0$.

In order to take into account the broadband spectrum of the STM-excited plasmon wave, equation 1 must be summed over the different wavelengths existing in the experimental data, while taking into account the relative intensities. This then yields

$$I_{tot}(k_x) = \sum_\lambda \left(\frac{J_1(u(\lambda))}{u(\lambda)}\right)^2 \Big[I_1(\lambda) + I_2(\lambda) + 2\sqrt{I_1(\lambda)I_2(\lambda)} * \cos\left(k_x(\lambda)d + k'_{SPP}(\lambda)(r_2 - r_1)\right)\Big] \quad (2)$$

If the intensity at the first hole is normalized to unity, i.e., $I_1 = 1$, the intensity at the second hole may be estimated by

$$I_2 = \frac{r_1}{r_2} e^{-2k''_{SPP}(r_2 - r_1)} \quad (3)$$

where k''_{SPP} is the imaginary part of the plasmon wavevector. In other words, as the plasmon wave travels from the first to second hole, part of the plasmon energy is dissipated in the gold sample and these losses are wavelength dependent as they are related to the imaginary component of plasmon wavevector k''_{SPP}. As k''_{SPP}

increases with decreasing wavelength (as the energy approaches the interband transitions in Au), the "bluer" components die out and the spectrum shifts to the red during propagation. This estimation for I_2 with respect to I_1 has been verified experimentally in Fig. 3. The blue curve is the normalized spectrum measured from the hole nearest to the STM tip and the red curve is the spectrum measured simultaneously at the second hole (this measured intensity has been divided by the maximum intensity from the first hole). If the cyan curve in Fig. 3 is the assumed spectrum from the first hole, equation 3 produces the magenta curve plotted in the same figure, agreeing well in both amplitude and wavelength with the experimental data.

Using equation 2, different features of the fringe pattern observed in Fig. 2 may be understood. The envelope has two origins: diffraction of the light scattered by the holes, and—that which interests us most here—the temporal coherence of the source. The decrease in the visibility away from the center of the fringe pattern is due to the source bandwidth. The non-unity visibility in the center of the fringe pattern, however, arises mainly from the unequal intensities at hole 1 and hole 2 discussed above. Finally, the very small change in the visibility observed for a large change in the spectrum (see Fig. 2) may be understood as follows: since the light from plasmons scattered at 1 μm-diameter holes arrives at large angle, the light from hole 1 travels farther to the back focal plane than the light from hole 2. This "extra" path difference due to high angle scattering almost cancels out the plasmon path difference that arises from the propagation of plasmons from hole 1 to hole 2. Thus, since the total path difference is very small, there is little change in the observed visibilities, despite the greater than tenfold difference in bandwidth. The asymmetry observed in the fringe pattern confirms that the total path difference is not strictly zero.

Equation 2 has been used to produce the blue curves of Fig. 2 c), d), g) and h). This simulation uses the experimental parameters including the emission spectrum of Fig. 3. The excellent fit to the data demonstrates several points: first of all, there is no loss of plasmon coherence upon scattering at holes (no matter whether the scattering be into photons or plasmons); this is important in applications involving extraordinary optical transmission[18]; second, besides the well-known and predictable plasmon decay in the lossy metal, no other inelastic loss in coherence may be attributed to SPP propagation; third, the good agreement between model and data suggests that there are no elastic dephasing processes present in the system; finally, the fact that the model consists of the overlapping of fringes of different wavelengths means that the coherence time may be estimated from the measured optical spectrum using the expression $\tau_c = \sqrt{\frac{2\ln 2}{\pi}}\frac{1}{\Delta\nu}$ with $\Delta\nu$ the spectral bandwidth of the Gaussian source[11]. Thus we have a coherence time τ_c on the order of 5-10 fs for STM-excited plasmons on gold (V_{sample}= 2.8 V). In order to directly measure the coherence time, subwavelength-diameter holes should be used to minimize the effects of diffraction and forward scattering on the interference pattern.

In conclusion, we have performed a variant of Young's double slit experiment in a specific geometry using a local, broadband, STM-plasmon source in order to investigate the temporal coherence of propagating surface plasmons. Comparing the results as a function of bandwidth to a model gives rise to the conclusion that when the effect of wavelength-dependent plasmon decay in the metal is taken into account, there is no further loss of coherence due to SPP propagation, SPP scattering at holes, or other dephasing processes. This result is important for future applications in plasmonics involving coherence, such as active communication devices.

We thank J.J. Greffet for fruitful discussions and J.F. Motte of the NANOFAB, Institut Néel, Grenoble for samples. This work is supported by the ANR project NAPHO (contract ANR-08-NANO-054) and the European STREP ARTIST (contract FP7 243421).

References

[1] R. Kolesov, B. Grotz, G. Balasubramanian, R. J. Stoehr, A. A. L. Nicolet, P. R. Hemmer, F. Jelezko, and J. Wrachtrup, Nat. Phys. **5**, 470 (2009).
[2] R. W. Heeres, L. P. Kouwenhoven, and V. Zwiller, Nat Nano **8**, 719 (2013).
[3] J. S. Fakonas, H. Lee, Y. A. Kelaita, and H. A. Atwater, Nature Photonics **8**, 317 (2014).
[4] G. Di Martino, Y. Sonnefraud, M. S. Tame, S. Kéna-Cohen, F. Dieleman, S. K. K. Oezdemir, M. S. Kim, and S. A. Maier, Phys. Rev. Applied **1**, 034004 (2014).
[5] N. Kuzmin, G. W. T. Hooft, E. R. Eliel, G. Gbur, H. F. Schouten, and T. D. Visser, Opt. Lett. **32**, 445 (2007).
[6] C. H. Gan, G. Gbur, and T. D. Visser, Phys. Rev. Lett. **98**, 043908 (2007).
[7] S. Aberra Guebrou, J. Laverdant, C. Symonds, S. Vignoli, and J. Bellessa, Opt. Lett. **37**, 2139 (2012).
[8] A. Caze, R. Pierrat, and R. Carminati, Phys. Rev. Lett. **110**, 063903 (2013).
[9] J. Laverdant, S. A. Guebrou, F. Bessueille, C. Symonds, and J. Bellessa, J. Opt. Soc. Amer. A **31**, 1067 (2014).
[10] T. Wang, E. Boer-Duchemin, G. Comtet, E. Le Moal, G. Dujardin, A. Drezet, and S. Huant, Nanotechnology **25**, 125202 (2014).
[11] J. W. Goodman, *Statistical Optics* (Wiley, 1985).
[12] B. J. Thompson, J. Soc. Photo. Inst. Engr. **4**, 7 (1965).
[13] T. Wang, E. Boer-Duchemin, Y. Zhang, G. Comtet, and G. Dujardin, Nanotechnology **22**, 175201 (2011).
[14] T. Wang, Ph.D. thesis, Univ. Paris-Sud, Orsay (2012).
[15] C. Sonnichsen, T. Franzl, T. Wilk, G. von Plessen, J. Feldmann, O. Wilson, and P. Mulvaney, Phys. Rev. Lett. **88**, 077402 (2002).
[16] D. S. Kim, S. C. Hohng, V. Malyarchuk, Y. C. Yoon, Y. H. Ahn, K. J. Yee, J. W. Park, J. Kim, Q. H. Park, and C. Lienau, Phys. Rev. Lett. **91**, 143901 (2003).
[17] O. Mollet, G. Bachelier, C. Genet, S. Huant, and A. Drezet, J. Appl. Phys. **115**, 093105 (2014).
[18] C. Genet and T. W. Ebbesen, Nature **445**, 39 (2007).